Materials Today Bio 14 (2022) 100243

Contents lists available at ScienceDirect

Materials Today Bio

journal homepage: www.journals.elsevier.com/materials-today-bio

Electrospun strong, bioactive, and bioabsorbable silk fibroin/poly (L-lactic-acid) nanoyarns for constructing advanced nanotextile tissue scaffolds

Jiao Liu [a,1], Tao Li [a,1], Hao Zhang [c], Wenwen Zhao [c], Lijun Qu [a,b], Shaojuan Chen [a], Shaohua Wu [a,b,*]

[a] College of Textiles & Clothing, Qingdao University, Qingdao, China
[b] Research Center for Intelligent and Wearable Technology, Qingdao University, Qingdao, China
[c] Qingdao University Medical College, Qingdao University, Qingdao, China

ARTICLE INFO

Keywords:
Electrospinning
Textile-forming technique
Nanotextile scaffolds
Nanofibrous yarns
Subcutaneous implantation

ABSTRACT

Bio-textiles have aroused attractive attentions in tissue engineering and regenerative medicine, and developing robust, bio-absorbable, and extracellular matrix (ECM) fibril-mimicking nanofibrous textiles is urgently required for the renewal of existing microfibrous textile-based scaffolds and grafts. In this study, an integrated electrospinning system consisting of one nanoyarn-forming unit and one hot stretching unit is reported to fabricate silk fibroin (SF)/poly (L-lactic-acid) (PLLA) nanofibrous yarns (nanoyarns). The hot stretching process is demonstrated to significantly improve the fiber alignment, crystallinity, and mechanical properties of SF/PLLA nanoyarns, compared to the unstretched controls. For instance, the fiber alignment degree of hot stretched 50/50 SF/PLLA nanoyarn has increased by 25%, and the failure strength has increased by 246.5%, compared with the corresponding un-stretched control. Increasing the SF/PLLA mass ratio is found to significantly decrease the crystallinity and mechanical properties, but notably increase the degradation rate and surface hydrophilicity of SF/PLLA nanoyarns. Different SF/PLLA nanoyarns are further meticulously interwoven with warp and weft directions to obtain several nanofibrous woven textiles. The results from *in vitro* cell characterization and *in vivo* subcutaneous implantation show that increasing the SF/PLLA mass ratio significantly improves the biological properties and effectively reduces the inflammatory response of nanoyarn-constructed textiles. Overall, this study demonstrates that our SF/PLLA nanoyarns with controllable physical, mechanical and biological performances are fantastic candidates for the designing and development of advanced nanoarchitectured textile tissue scaffolds.

1. Introduction

In recent years, biomedical textiles have received attractive attentions in the fields of tissue engineering and regenerative medicine, originated from their adjustable 3D porous structure, appropriate integration of softness and hardness, and ideal biological properties [1,2]. Biomedical textiles are commonly designed and implemented by interlacing fiber-constructed yarns with various textile technique (i.e., weaving, knitting, and braiding). The fibrous yarns with predetermined properties are considered to be the primary configuration unit for the construction of bio-textiles, which notably influence the structure and performances of finally obtained bio-textiles.

The directed conversion of electrospun nanofibers into yarn-like structure has opened a new window to manufacture innovative nanoyarns made from nanofibers with the diameters ranging from several to several hundred nanometers [3,4]. The electrospun nanoyarns with high specific surface area and high aspect ratio have been demonstrated to provide more cell adhesion sites in comparison with the traditional textile yarns made from micro-sized fibers (fiber diameter≥10 μm) [5,6]. Moreover, the nanofibers existed in the electrospun nanoyarns are found to effectively simulate the fiber scale and hierarchical structure of protein fibers in the native extracellular matrix (ECM). These characteristics are all beneficial for the repair and regeneration of damaged or injured tissues, which make the electrospun nanoyarns as potential candidates for

* Corresponding author. College of Textiles & Clothing, Qingdao University, Qingdao, China.
E-mail address: shaohua.wu@qdu.edu.cn (S. Wu).
[1] These authors contribute equal to this manuscript.

https://doi.org/10.1016/j.mtbio.2022.100243
Received 23 January 2022; Received in revised form 10 March 2022; Accepted 12 March 2022
Available online 24 March 2022

the development of textile-based scaffolds and grafts [4,7,8]. However, there are still some severe drawbacks and limitations, such as uncontrollable physical structure, inferior mechanical performance, as well as inappropriate biochemical component, which hold back the practical applications of electrospun nanoyarns.

One of the most important aspects for the fabrication of nanoyarns is to improve the physical structure. As known that, the native ECMs existed in plenty of tissues, such as tendon [9,10],blood vessel [11,12], nerve [13,14], as well as muscle [15,16], possess highly aligned nanofibrous structures, which are deemed to be an extremely pivotal factor for controlling and regulating the formation of anisotropic architecture in the corresponding tissues. Although there are several approaches that have been reported to directly assemble electrospun nanofibers into nanoyarns, it is still a huge challenge to develop the nanoyarns with highly aligned nanofibrous structure and receivable yarn evenness [17–20].

The appropriate mechanical properties are also significantly important for the fabrication of electrospun nanoyarns. It is well known that sufficient mechanical properties are the prerequisite conditions to implement the textile yarns into various applications [1,21]. Twisting process has been widely utilized to enhance the cohesive force between fibers in the yarn texture, further resulting in the increase of the mechanical properties of textile yarns in the traditional textile industry [22,23]. It is demonstrated that the twisted nanoyarns present better mechanical properties than the untwisted nanoyarns [24,25]. However, compared with the traditional textile yarns, the prepared twisted nanoyarns are only equivalent to raw filament, which are still unsatisfied for the usage of biotextile fabrication. What is worse, the introduced twisting process can notably break the fiber alignment of electrsopun nanoyarns, which negatively influence the control and regulation of cell behaviors and tissue regeneration of nanoyarn-based biotextiles.

The composition of electrospun nanoyarns is another important factor that affects biological properties of the biotextiles. Due to the excellent inclusiveness of electrospinning, a variety of natural and synthetic polymers have been electrospun into nanofiber-contained webs and yarns. Natural polymers mainly include silk fibroin (SF), collagen (COL), chitosan (CS), and hyaluronic acid (HA) etc., which commonly possess a large number of bioactive sites and polymer modification sites but exhibit poor mechanical performance and unavailable processibility [26–29]. In contrast, synthetic polymers, such as poly (L-lactic acid) (PLLA), polylactic-co-glycolic acid (PLGA), poly (L-lactide--co-ε-caprolactone) (PLCL), and polydioxanone (PPDO), usually have tunable biodegradability, high mechanical property, and distinguished workability [28,30–32]. Consequently, a combined use of the natural polymers and synthetic polymers is assuredly necessary for electrospun nanoyarns, which not only encompasses the biological properties, but also retains splendid mechanical properties and processibility.

In the present study, a novel integrated electrospinning system which combines nanoyarn-forming process with hot stretching process is designed and developed to fabricate nanoyarns. The hot stretching process is expected to improve physical structure, enhance mechanical properties, and increase biological properties of nanoyarns. One natural polymer (SF) and one synthetic polymer (PLLA) with different mass ratios are chosen as raw materials to fabricate several different types of nanoyarns. The morphology, structure, physical and mechanical properties of as-prepared different SF/PLLA nanoyarns with/without hot stretching are systematically explored. The different hot stretched SF/PLLA nanoyarns are further explored as primary building units to manufacture advanced nanostructured woven fabrics by textile weaving technique. Both *in vitro* cell characterizations and *in vivo* subcutaneous embedding characterizations are carried out to investigate and compare the biological properties of as-fabricated different SF/PLLA woven fabrics. The present study is expected to provide some guidance and reference for the innovated design and development of SF/PLLA nanoyarns to construct adjustable nanostructured woven fabrics for soft tissue engineering applications.

2. Experimental

2.1. Materials

PLLA ($M_W = 100{,}000$ Da) powders were obtained from Jinan Daigang Biomaterial (China). Bombyx mori silk cocoons were provided by Sheng Tianyi Trading (China). Sodium carbonate, Lithium bromide, and 1, 1, 1, 3, 3-Hexafluora-2-propanol (HFIP, $M_W = 168.04$ Da) were purchased from Aladdin reagents (China) and used as received.

2.2. Preparation and extraction of SF

SF was extracted following our previous experimental protocols [33,34]. Briefly, Bombyx mori silk cocoons were cut into dime-sized pieces that were degummed with boiling sodium carbonate solution, and the as-degummed silk materials were squeezed and dried overnight in room temperature. After that, they were dissolved with the 9.3 M lithium bromide solution to prepare an amber SF solution. After further dialyzed for about 48 h and centrifugated two times at 4 °C with a speed of 9000 rpm, the pure SF solution was obtained and frozen at −80 °C overnight. Eventually, the as-frozen SF materials were lyophilized to totally remove the solid water, and the completely-dried SF materials were obtained, and stored at −20 °C before further use.

2.3. Fabrication of SF/PLLA nanoyarns

Four different types of nanoyarns made from adjustable SF/PLLA mass ratios were manufactured by using our modified electrospinning system, which was constructed with one nanoyarn-forming unit and one hot stretching unit (Fig. 1(a)). Firstly, SF/PLLA with the different mass ratios including 0/100, 20/80, 35/65 and 50/50 were dissolved into HFIP solvent to prepare a series of homogeneous spinning solutions with a fixed polymeric concentration of 10% (w/v), respectively. The as-prepared polymeric solutions were further loaded into two 10 mL syringes with 18 G blunt needles, which were laid oppositely at a distance of 20 cm. The solution flow rates were both maintained at 0.8 mL/h with two syringe pumps. A high voltage supply was utilized to emit positive and negative voltages (±12 kV) to two oppositely-deposited needles, respectively, which produced both positively and negatively charged nanofibers simultaneously. A nanofiber buncher composed of with one neutral metal disc (NMD) and one neutral hollow metal rod (NHMR) was employed to collect the nanofibers. The NMD and NHMR was placed with an interval distance of 10 cm, and deposited in the same plane perpendicular to two syringes. The NMD rotated with a speed of 250 rpm to make the as-collected nanofibers form a stable spinning triangle cone, resulting in the generation of nanoyarns. The raw nanofiber yarns were drawn in a hot stretching unit of 80 °C for roughly 30 s, and the hot-stretched nanofiber yarns with a draw ratio of 2 were obtained.

2.4. Morphological characterization of SF/PLLA nanoyarns

The morphology of as-obtained nanoyarns with various SF/PLLA ratios was visualized by a scanning electron microscope (SEM, TESCAN VEGA3, Czech Republic) with an accelerated voltage of 10 kV. All samples were coated with a thin layer of gold before the SEM observation. An Image J software (National Institutes of Health, USA) was utilized to analyze the mean yarn diameter, the mean fiber diameter, and the fiber orientation distribution (relative to horizontal axis). Randomly selected 100 nanofibers from 5 SEM images were employed to measure the mean fiber diameter and the fiber orientation distribution, and more than 50 data points based on 5 SEM images were randomly chosen to calculate the mean yarn diameter.

2.5. FTIR, XRD and DSC analysis of SF/PLLA nanoyarns

A Fourier transform infrared (FTIR) spectrometer (Thermo Fisher

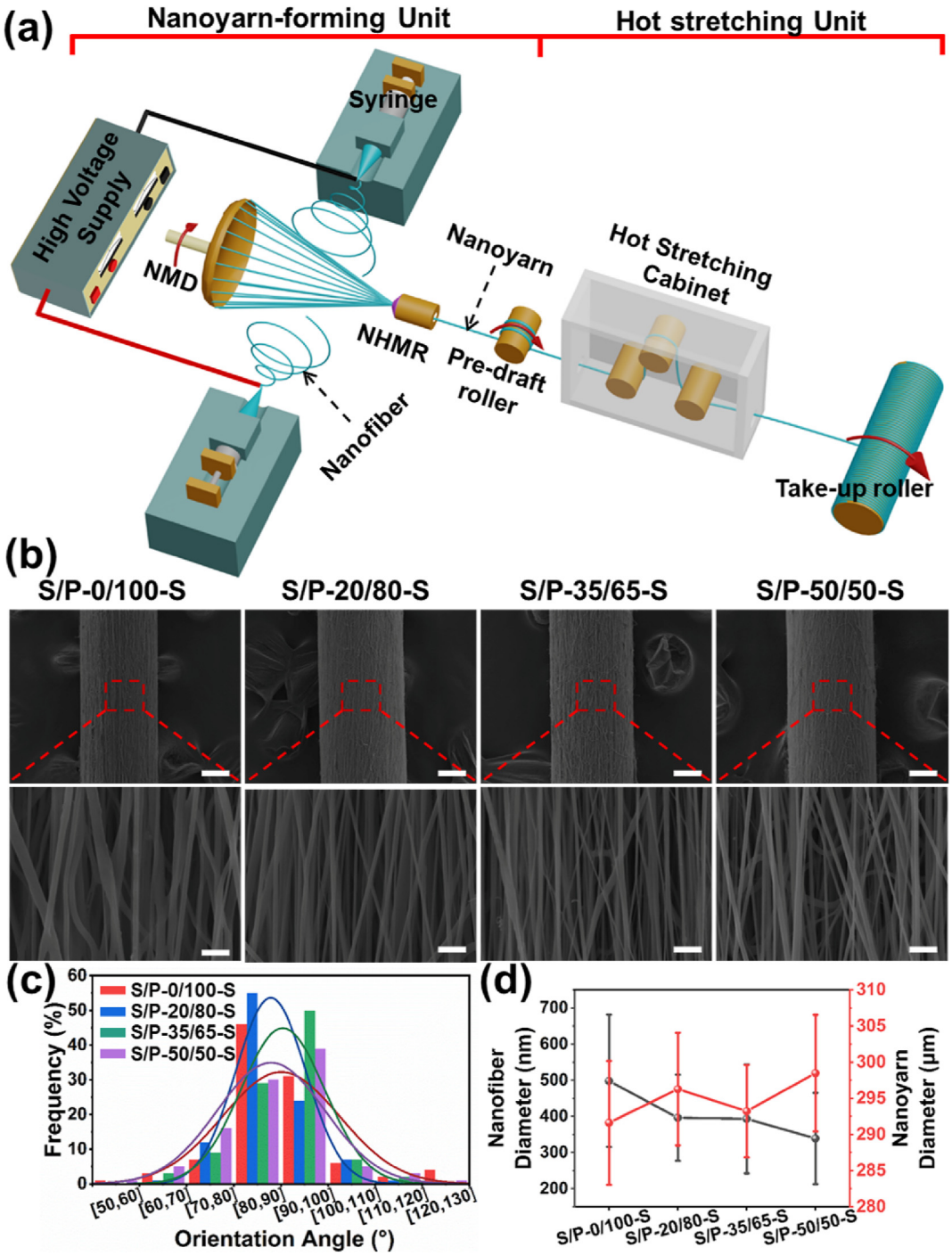

Fig. 1. Preparation and morphological characterization of nanoyarns with different SF/PLLA mass ratios. (a) Schematic of novel electrospinning system with one nanoyarn-forming unit and one hot stretching unit. (b) SEM images of four different hot stretched SF/PLLA nanoyarns. Scale bars for top panel: 100 μm. Scale bars for bottom panel: 2.5 μm. Quantitative analysis of (c) fiber orientation angular distribution and (d) yarn diameter and nanofiber diameter in four different hot stretched SF/PLLA nanoyarns.

Scientific 5225 Verona RD, USA) was employed to determine the chemical groups of all the different SF/PLLA nanoyarns. All the FTIR spectrums were scanned with a 4 cm^{-1} resolution ranging from 4000 cm^{-1} to 400 cm^{-1}. The X-ray diffraction (XRD) spectroscopy of all the SF/PLLA nanoyarns was determined by a Rigaku Ultima IV machine with a Cu Kα radiation source (Japan). The operating voltage and current were kept at 40 kV and 40 A. Each sample was detected from 5° to 60° (2θ) with a scanning rate of 5° (2θ) per minute. A DSC2500 tester (TA Instruments, USA) was used to determine thermal performances of all the different SF/PLLA nanoyarns. Each sample with a mass of ~6 mg was heated from 30 °C to 250 °C at a scanning rate of 10 °C/min under a nitrogen atmosphere.

2.6. Mechanical test of SF/PLLA nanoyarns

The mechanical properties of all the SF/PLLA nanoyarns with different mass ratios were measured using a tensile testing machine (Instron-3300 Tensile Machine, Glenview, USA). For all the specimens, the clamping distance and tensile rate were maintained at 20 mm and 10 mm/min, respectively. Before the formal tensile testing, 0.02 N pre-

tension was applied to eliminate the test deviation. The load-elongation curves were firstly obtained, and then four important mechanical parameters including the breaking load, breaking elongation, Young's modulus as well as ultimate strength were calculated.

2.7. In vitro degradation experiments of SF/PLLA nanoyarns

The hot stretched SF/PLLA nanoyarns with different mass ratios were weighed, then immersed in the phosphate-buffered saline (PBS) solution (pH = 7.4) in a 37 °C oscillator (SHZ-88A, China) with a speed of 100 rpm. The PBS and nanoyarns were collected according to the predetermined time points (1, 2, 3, 4, 5, 6, 7 and 8 weeks). The nanoyarn morphology after the degradation was observed using SEM, and a pH meter (FE28-Meter, Switzerland) was utilized to measure the pH value of PBS solution after nanoyarn degradation. The mass loss rate (%) was calculated using the following formula:

$$\text{Mass loss rate } (\%) = \frac{Mo - M}{Mo} \times 100\%$$

where M_o is the original mass of nanoyarns, M is the mass of corresponding nanoyarns at the pre-set degradation time point.

2.8. Fabrication of SF/PLLA woven fabrics

All the hot stretched SF/PLLA nanoyarns with different mass ratios were utilized as both warp and weft yarns, and interwoven in an orthogonal manner to generate the diverse woven fabrics with the plane weaving pattern. The warp density and weft density for all the fabric fabrication were fixed at 70 yarns/10 cm and 220 yarns/10 cm, respectively. The SEM was employed to observe the morphology of fabricated woven fabrics after the gold coating process. An Image J software was utilized to determine the pore size of each woven fabric.

2.9. Surface hydrophilicity and mechanical characterizations of SF/PLLA woven fabrics

The surface hydrophilicity of different SF/PLLA woven fabrics was determined by a video water contact angle machine (KRUSS, Drop shape analyser-DSA25, Germany). A 2 μL deionized water droplet was put onto the surface of different woven fabrics, and the water contact angle was visualized and recorded after the water droplet was totally balanced on the fabric samples. The mechanical properties of different SF/PLLA woven fabrics along with two directions, i.e., warp direction and weft direction, were determined by using an Instron-3300 Tensile Machine. The testing parameters were kept the same with the above-mentioned mechanical test of SF/PLLA nanoyarns.

2.10. In vitro cell seeding and culture

Human adipose-derived mesenchymal stem cells (HADMSCs, cell bank, Chinese Academy of Sciences) were cultured in a medium containing DMEM/F12 medium (Gibco), 10% fetal bovine serum (FBS, Gibco), and 1% penicillin/streptomycin (P/S, Gibco). The cells were incubated in a 5% CO_2-contained incubator at 37 °C. All the woven fabrics made from different SF/PLLA nanoyarns were cut into a size of 10 mm × 10 mm, and sterilized with ultraviolet light irradiation for 2 h, and then treated with 70% (v/v) ethanol overnight. Subsequently, the as-sterilized woven fabrics were washed 3 times with sterilized PBS solution and submerged in a culture medium overnight. Thereafter, 20 μL of 1×10^5 HADMSCs were seeded on each fabric specimen and incubated to the predetermined time point. The culture medium was replaced every two days.

2.11. Cell morphology and proliferation characterization

After 7 days of culture, all the cell-fabric constructs were fixed in 4% paraformaldehyde for 4 h, and penetrated using 0.2% Triton-X100 in PBS for 10 min, and further obstructed with 1% bovine serum albumin (BSA) overnight at 4 °C. Each cell-fabric construct was stained with IFluorTM 488 phalloidin dye (Yeasen Biotechnology Co., Ltd., China) for 2 h at room temperature in the dark, and then stained with DAPI (Yeasen Biotechnology Co., Ltd., China) for 30 min at room temperature in the dark. After that, all the cell-fabric samples were observed using a confocal laser scanning microscope (CLSM, Zeiss 900 CLSM). An Image J software was utilized to count the cell number from random fields of view (FOV) on three different fabrics for each specimen. The cell-fabric constructs after 7-day culture were washed once with PBS solution to remove the unattached cells and fixed in 0.2% glutaraldehyde for 60 min at 4 °C. Then the samples were dehydrated in a series of ethanol with 30%, 50%, 70%, 80%, 90%, 100% gradient. The samples were completely dried, and observed using SEM after the gold spraying process. An MTT assay kit (Solarbio, China) was utilized to quantitatively evaluate the cell proliferation after 4 h, 1 day, 3 days and 7 days of culture, respectively. At the predetermined time point, the cell-fabric constructs were soaked in the MTT solution and incubated for 4 h to obtain the purple formazan crystals according to the manufacturer's instruction, then dissolved with dimethyl sulfoxide (DMSO, Solarbio, China) to obtain the purple solution. Eventually, the absorbance value was read and recorded at the wavelength of 490 nm using a microplate reader (Infinite M Nano, Tecan).

2.12. In vivo subcutaneous implantation

The *in vivo* subcutaneous implantation was carried out strictly following the protocol approved by the Animal Care and Experiment Committee of Qingdao University. 12 male Sprague-Dawley rats were randomly divided into 4 groups for implantation of the woven fabrics with different SF/PLLA ratios: SF/PLLA-0/100 woven fabrics (n = 3), SF/PLLA-20/80 woven fabrics (n = 3), SF/PLLA-35/65 woven fabrics (n = 3), and SF/PLLA-50/50 woven fabrics (n = 3). Briefly, the surgery was performed under anaesthesia, and the rat skin on the dorsal region was shaved. After that, one midline incision was created, and a blunt dissection method was utilized to generate two oppositely-deposited subcutaneous pockets through the incision. The woven fabrics with a size of 10 mm × 10 mm were implanted and embedded into the pocket, and then sutured and disinfected. The as-operated rats were maintained under a 12 h light/dark cycle and allowed to have food and water in a freedom manner. After 14 days of surgical operation, the rats were sacrificed and the woven fabrics with the surrounding tissues were harvested for the further evaluation and analysis.

2.13. Histological analysis

The retrieved woven fabrics with the surrounding tissues were fixed in 10% formalin solution for 48 h, and dehydrated with different concentrations of ethanol, and then embedded in paraffin. The as-embedded tissue specimens were sectioned into a series of slides with 5 μm thickness along with the cross-sectional direction of implanted woven fabrics by a microtome (SM2500, Leica, Nussloch, Germany). Some slides were treated with hematoxylin and eosin (H&E) staining and Masson's trichrome (M&T) staining, respectively, and observed under a microscopy (Inverted fluorescence microscope, Zeiss Imager. M2). Moreover, some slides were double stained with CD68 antibody (Bioss, China) and DAPI (Yeasen, China), and observed with a Zeiss 900 CLSM, in order to investigate the inflammation response of four different SF/PLLA woven fabrics. An Image J software was utilized to calculate the thickness of capsuled collagen layer based on M&T staining and the fluorescent density of CD68-positive immune-reactivity based on immunofluorescent staining. A biological technician, totally unaware of this experiment, was

required to select the detection threshold, and the threshold level was fixed at the same once chosen. Three images were randomly chosen from three different replicates to determine the mean value for each specimen.

2.14. Statistical analysis

All quantitative data were expressed as mean ± standard deviation (SD). All the experiments in this study were performed at least 3 replicates for each group. Statistical analysis was performed using ANOVA with Scheffé post-hoc tests. A value of $p < 0.05$ is considered to have statistically significant difference.

3. Results and discussion

3.1. Fabrication and morphological characterization of SF/PLLA nanoyarns

An integrated electrospinning system containing one nanoyarn-forming device and one hot stretching apparatus was designed and developed to manufacture a series of nanoyarns with different SF/PLLA mass ratios (Fig. 1(a)). To explore the effects of hot stretching process on the morphology and structure of fabricated nanoyarns, the SF/PLLA nanoyarns with and without hot stretching were fabricated and investigated. The as-spun raw nanoyarns without hot stretching process were named as S/P-0/100-R, S/P-20/80-R, S/P-35/65-R and S/P-50/50-R, respectively, according to the different SF/PLLA mass ratio (SF/PLLA = 0/100, 20/80, 35/65, and 50/50). For the corresponding nanoyarns experienced one fold of hot stretching in a hot stretching device with the temperature of 80 °C, the finally-obtained nanoyarns were named as S/P-0/100-S, S/P-20/80-S, S/P-35/65-S, and S/P-50/50-S, respectively. Fig. 1(b) showed the SEM images of hot stretched nanoyarns with diverse SF/PLLA mass ratios, and Supplemental Fig. S1(a) displayed the SEM images of the corresponding raw nanoyarns without the hot stretching treatment. It was found that the internal nanofibers existed in all the nanoyarns with/without hot stretching presented smooth morphology and no bead-like defects were observed. The statistical analysis showed that the hot stretching process significantly improved the fiber alignment of nanoyarns. The frequency of fiber orientation angle in the range from 80° to 100° accounted for ~46%, 44%, 48% and 44% for S/P-0/100-R, S/P-20/80-R, S/P-35/65-R, and S/P-50/50-R nanoyarns, respectively (Supplemental Fig. S1(b)). In comparison, ~77%, 79%, 79%, and 69% of fibers exhibited the orientation angel in the range of 80°–100° for S/P-0/100-S, S/P-20/80-S, S/P-35/65-S, and S/P-50/50-S nanoyarns, respectively (Fig. 1(c)).

The fiber diameter analysis displayed that the mean fiber diameter of the S/P-0/100-R, S/P-20/80-R, S/P-35/65-R, and S/P-50/50-R nanoyarns was 796 ± 255 nm, 514 ± 174 nm, 411 ± 110 nm, and 387 ± 157 nm, respectively (Supplemental Fig. S1(c)). The results indicated that the fiber diameter of nanoyarns presented a decreased trend with the increase of SF content, mainly due to the different SF/PLLA ratios of different spinning solutions. Some other studies also found the nanofiber diameters presented a decreased trend with the increasing of SF/PLLA ratio during the electrospinning of a blend of SF and PLLA, attributed to the obviously changed solution properties [35–37]. In contrast, the obviously decreased fiber diameter was found in the hot stretched nanoyarns (498 ± 183 nm for S/P-0/100-S, 396 ± 119 nm for S/P-20/80-S, 393 ± 151 nm for S/P-35/65-S, and 339 ± 126 nm for S/P-50/50-S (Fig. 1(d)). The hot stretched nanoyarns also presented notably lower mean yarn diameter in comparison with the counterparts without hot stretching. Talking together, the nanofiber diameters decreased with the increasing of SF/PLLA ratio, and the hot stretching also could effectively reduce the nanofiber diameters.

Several previous studies demonstrated that the physical structure of electrospun nanoyarns could be improved by adjusting the distribution of electric field and/or changing the morphology and architecture of gathering device [20,21]. In the present study, a relatively simple hot stretching process was introduced into our modified electrospinning nanoyarn-forming system and demonstrated that the hot stretching process significantly improved the fiber alignment of nanoyarns. For instance, the fiber alignment degree of hot stretched S/P-0/100, S/P-20/80, S/P-35/65, and S/P-50/50 nanoyarns had increased 31%, 35%, 31% and 25%, respectively, compared with the corresponding un-stretched S/P-0/100, S/P-20/80, S/P-35/65, and S/P-50/50 nanoyarns. During the hot stretching process, the inner molecular chains began to move once the temperature exceeded the glass transition temperature, leading to the re-orientation of macromolecular chains and internal non-oriented crystals along with the force application direction [38]. These phenomena were doubtlessly instructive for the improvement of fiber alignment and the formation of new crystals of finally-obtained yarns.

3.2. FTIR, XRD and DSC analysis and mechanical properties of SF/PLLA nanoyarns

The FTIR spectra of different SF/PLLA nanoyarns with/without hot stretching were displayed in Fig. 2(a) and Supplemental Fig. S2(a). A relatively wide weak peak at ~2998 cm^{-1} belonged to the asymmetric stretching vibration of -C-H, and a strong peak at ~1756 cm^{-1} was ascribed to the stretching vibration of the –C═O. One peak at ~1084 cm^{-1} was responsible for the stretching vibration of -C-O. All these three characteristic peaks originated from PLLA polymer were detected in all the SF/PLLA nanoyarns with/without hot stretching. In addition, all the SF contained nanoyarns presented several characteristic peaks. Two peaks centered at ~1656 cm^{-1} and ~1538 cm^{-1} were attributed to the

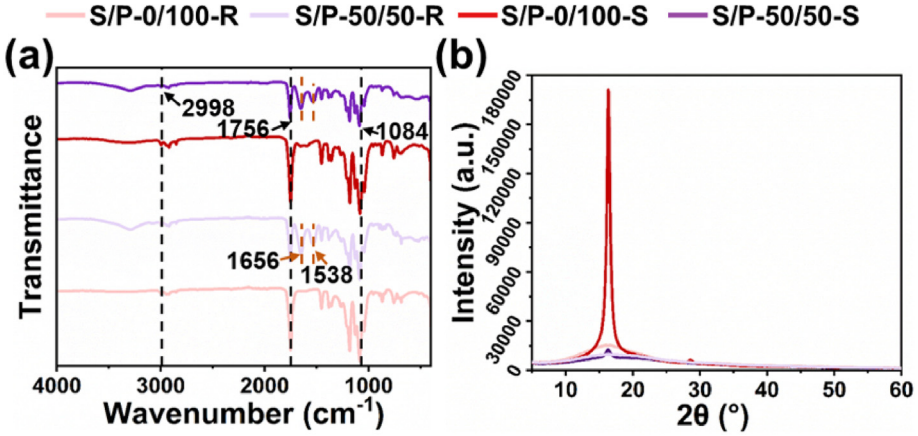

Fig. 2. Physical characterizations of S/P-0/100-R, S/P-50/50-R, S/P-0/100-S and S/P-50/50-S nanoyarns. (a) FTIR spectra and (b) XRD profiles.

amide region I and amide region II, which all belonged to the β-folded characteristic peak. It was found that the hot stretching process did not change the chemical groups of different SF/PLLA nanoyarns, and no obvious peak shifting phenomena were observed. Moreover, the results also demonstrated that the SF and PLLA components were only simply mixed in the nanoyarns, and no new chemical groups were generated during the processes of electrospinning and hot stretching. The XRD profiles of different SF/PLLA nanoyarns with/without hot stretching were shown in Fig. 2(b) and Supplemental Fig. S2(b). The four stretched nanoyarns including the S/P-0/100-S, S/P-20/80-S, S/P-35/65-S, and S/P-50/50-S nanoyarns exhibited an obvious diffraction peak centered at ~16.4°, corresponding to the 110/200 planes of α′ form crystalline of PLLA polymer. As control, a notably lower diffraction peak at ~16.4° was detected for the four corresponding SF/PLLA nanoyarns without hot stretching, i.e., the S/P-0/100-R, S/P-20/80-R, S/P-35/65-R, and S/P-50/50-R nanoyarns. The results indicated that the introduced hot stretching process could significantly improve the crystallinity of nanoyarns. The existing studies showed that the PLLA molecular chain could move and further re-shaped to form α′ crystals by hot stretching process [39–42]. In addition, the increase of SF content was found to significantly decrease the crystal peak of PLLA component, which may be attributed that the addition of SF could reduce the ordered arrangement of lactic units and weaken the crystal formation. The DSC curves of different SF/PLLA nanoyarns with/without hot stretching were shown in Supplemental Fig. S3(a), and the corresponding thermal parameters including glass transition temperature (T_g), melting temperature (T_m) and melting enthalpy (ΔH_m) were displayed in Supplemental Fig. S3(b). It was found that the hot stretching process obviously improved the T_g value of nanoyarns, and increasing the SF content also increased the T_g value of nanoyarns. In addition, the stretched yarns possessed notably increased ΔH_m value compared with the corresponding unstretched controls, and the increase of SF content was found to significantly

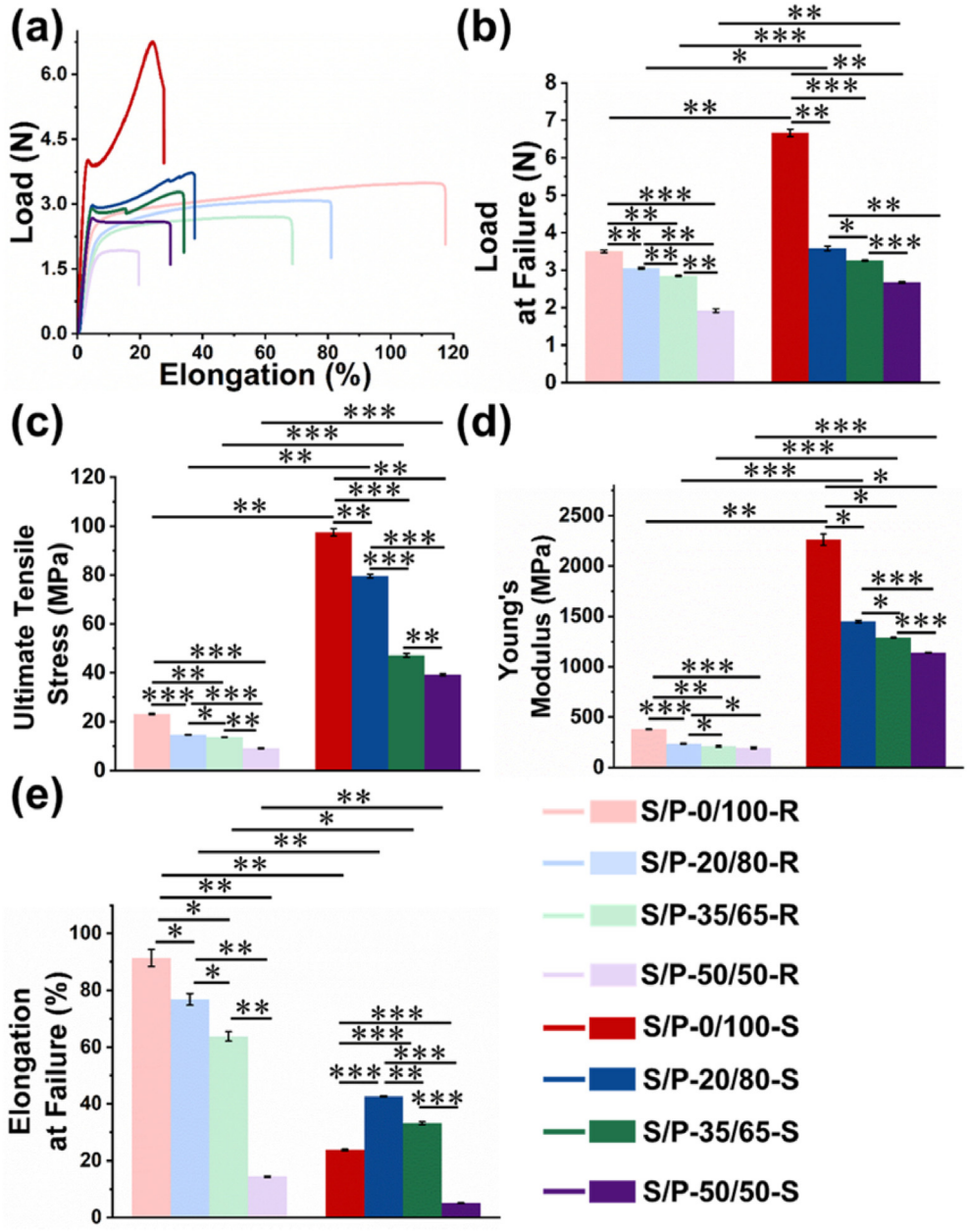

Fig. 3. Uniaxial tensile characterizations of eight different SF/PLLA nanoyarns with/without hot stretching. (a) Representative load–elongation curves. (b) Load at failure (n = 3; *p < 0.05, **p < 0.001, ***p < 0.0001). (c) Ultimate tensile stress (n = 3; *p < 0.05, **p < 0.001, ***p < 0.0001). (d) Young's modulus (n = 3; *p < 0.05, **p < 0.001, ***p < 0.0001). (e) Elongation at failure (n = 3; *p < 0.05, **p < 0.001, ***p < 0.0001).

decrease the ΔH_m value. As well known that the ΔH_m value can effectively reflect the crystallinity of polymeric samples. The ΔH_m calculation from DSC curves further confirmed the crystallinity analysis based on XRD curves.

Fig. 3(a) showed the representative load-elongation curves of different SF/PLLA nanoyarns with/without hot stretching. The four different SF/PLLA nanoyarns without hot stretching, i.e., the S/P-0/100-R, S/P-20/80-R, S/P-35/65-R, and S/P-50/50-R nanoyarns, exhibited a similar tensile behavior with an initial linear elastic region followed by a yield platform region until the failure occurred. The yield platform region was found to decrease dramatically with the increase of SF content. In contrast, the four different SF/PLLA nanoyarns with hot stretching, i.e., the S/P-0/100-S, S/P-20/80-S, S/P-35/65-S, and S/P-50/50-S nanoyarns, displayed notably different tensile curves. An obvious plastic deformation region was presented after a linear elastic region.

Four mechanics-related important parameters, including failure load, failure stress, Young's modulus and failure elongation, were calculated based on the load-elongation curves, and were displayed in Fig. 3(b) and (c). The results showed that all the four hot-stretched nanoyarns exhibited obviously improved failure load, failure stress, and Young's modulus, but notably decreased failure elongation, when compared with the four counterparts without hot stretching. We further compared the differences of mechanical properties among all the SF/PLLA nanoyarns with hot stretching. The statistical analysis showed that the failure load, failure stress, and Young's modulus significantly decreased as the SF content increased. More specifically, the failure stress of the hot stretched S/P-0/100, S/P-20/80, S/P-35/65, S/P-50/50 nanoyarns was 97.5 ± 1.5 MPa, 79.5 ± 0.8 MPa, 47.1 ± 0.7 MPa, and 39.2 ± 0.4 MPa, respectively, which have increased 322.2%, 446.7%, 246.5%, 326.8% compared with the corresponding un-stretched S/P-0/100, S/P-20/80, S/P-35/65, S/P-50/50 nanoyarns. The Young's modulus of hot stretched S/P-0/100, S/P-20/80, S/P-35/65, S/P-50/50 nanoyarns were 2662.6 ± 55.7 MPa, 1448.2 ± 12.1 MPa, 1290.5 ± 4.3 MPa, and 1139.1 ± 5.2 MPa, which have increased 600.7%, 543.1%, 513.1%, 482.4% than those un-stretched controls. The elongation at failure of hot stretched S/P-0/100, S/P-20/80, S/P-35/65, S/P-50/50 nanoyarns were 23.8 ± 0.3%, 37.7 ± 0.1%, 33.2 ± 0.5%, 25.9 ± 0.1%, which have decreased 284.0%, 103.7%, 92.2%, 188.0% in comparison with the corresponding un-stretched S/P-0/100, S/P-20/80, S/P-35/65, S/P-50/50 nanoyarns. Taken together, all these results indicated that the hot stretching process could effectively improve the mechanical properties of SF/PLLA nanoyarns, and the introduction of SF component could notably decrease the mechanical properties of SF/PLLA nanoyarns.

The ideal electrospun nanoyarns should also possess strong mechanical properties, which could not only maintain their structural stability, but also meet the fabrication requirement of diverse textile patterns. Many previous studies have demonstrated that the nanoyarns exhibited poor mechanical properties unless some post-treatments were utilized. The twisting process, a traditional textile technique, has been introduced into the electrospinning system in order to improve the nanoyarn mechanics. Two typical modified electrospinning methods including the dynamic liquid electrospinning system [24,43,44] and the conjugated electrospinning system [45–47] were derived and developed by inducing twisting mechanism in the electrospinning process. The

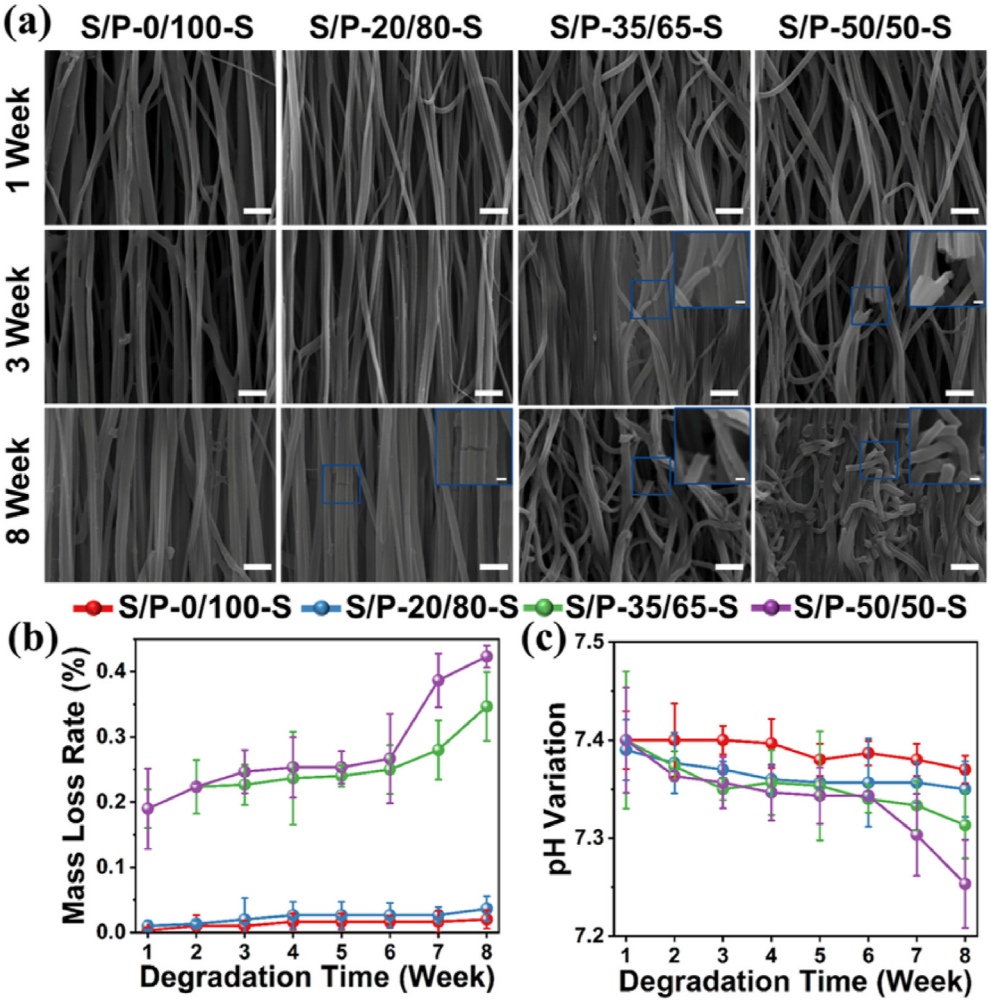

Fig. 4. *In vitro* degradation characterizations of hot stretched nanoyarns with different SF/PLLA mass ratio. (a) SEM observation at different predetermined time point throughout 8 weeks. Scale bars = 2.5 μm for SEM images, scale bars = 500 nm for inserted images with blue box. Quantitative measurements of mass loss rate (b) and pH value (c) at different predetermined time points throughout 8 weeks. (For interpretation of the references to color in this figure legend, the reader is referred to the Web version of this article.)

dynamic liquid electrospinning system employed the liquid vortex flowing as the driving force to twist the electrospun nanofibers into textile yarn-like structure. The conjugated electrospinning system utilized the rotating disk, rotating ring, or rotating cylinder to generate mechanical force, which further clustered and twisted the nanofibers into nanoyarns. Although the two above-mentioned twisting processes were demonstrated to improve the mechanical properties of electrospun nanoyarns to some extent, they severely damaged the fiber alignment structure of electrospun nanoyarns. Our study introduced an innovative hot stretching process, which could dramatically improve the fiber alignment and crystallinity of electrospun nanoyarns, resulting in enhanced mechanical properties. For instance, the failure stress of hot stretched S/P-0/100, S/P-20/80, S/P-35/65, and S/P-50/50 nanoyarns had increased 322.2%, 446.7%, 246.5% and 326.8%, respectively, compared with the corresponding un-stretched S/P-0/100, S/P-20/80, S/P-35/65, and S/P-50/50 nanoyarns. Some studies also demonstrated that the hot stretching process was beneficial to promote the fiber alignment and crystallinity, and further enhance the mechanical performances of micro-sized polymeric filaments in traditional textile industry [40,48–50]. The present study offered a new routine to fabricate electrospun nanoyarns, which not only possessed excellent mechanical properties, but also maintained high fiber alignment.

3.3. In vitro degradation of SF/PLLA nanoyarns

The *in vitro* degradation behaviors of four hot stretched SF/PLLA nanoyarns were characterized by observing morphology change, testing the mass loss rate and pH variation at predetermined time points (Fig. 4(a)). SEM images showed that the nanofibers existed in both S/P-35/65-S and S/P-50/50-S nanoyarns started to have obvious breaking points after 3 weeks of degradation (Fig. 4(b)). The nanofibers in S/P-20/80-S nanoyarns began to present exiguous break points at week 8. In comparison, the nanofibers in S/P-0/100 nanoyarns even did not show any fiber breaking points even after 8 weeks of degradation. The quantitative analysis displayed that the mass loss rate increased for all the four SF/PLLA nanoyarns as the degradation time increased. Both S/P-35/65-S and S/P-50/50-S nanoyarns presented significantly higher mass loss rate in comparison with S/P-0/100-S nanoyarns and S/P-20/80-S nanoyarns. We also found that the pH value lightly decreased for all the four SF/PLLA nanoyarns with the increase of degradation time, but still presented some visible differences among the four different nanoyarn groups (Fig. 4(c)). All these results demonstrated that the introduction of SF component could speed up the *in vitro* degradation rate. The previous study investigated the *in vitro* degradation electrospun SF/PLLA nanofibers without hot stretching and found that the degradation rate increased as the proportion of PLLA was decreased in the SF/PLLA nanofiber scaffold after 8 weeks of degradation [37]. Specifically, the mass loss rate of S/P-50/50 without hot stretching was found to be about 55% at week 8. As control, the hot stretched S/P-50/50 in our study presented an obviously lower mass loss rate (0.4%) at the same degradation period. This phenomenon can be attributed to the significantly increased crystallinity of S/P-50/50 after hot stretching (Fig. 2(b)).

3.4. Fabrication and in vitro cell characterizations of SF/PLLA nanoyarn-based woven fabrics

The textile weaving technique was further utilized to interlace four different hot stretched SF/PLLA nanoyarns into plain weaving patterns, respectively (Fig. 5(a)). The SEM images showed that all the SF/PLLA woven textiles exhibited similar uniform morphology and structure (Fig. 5(b)). The mean area of single pores was determined to be 0.917 ± 0.085 mm^2 for S/P-0/100-S woven fabric, 0.937 ± 0.071 mm^2 for S/P-

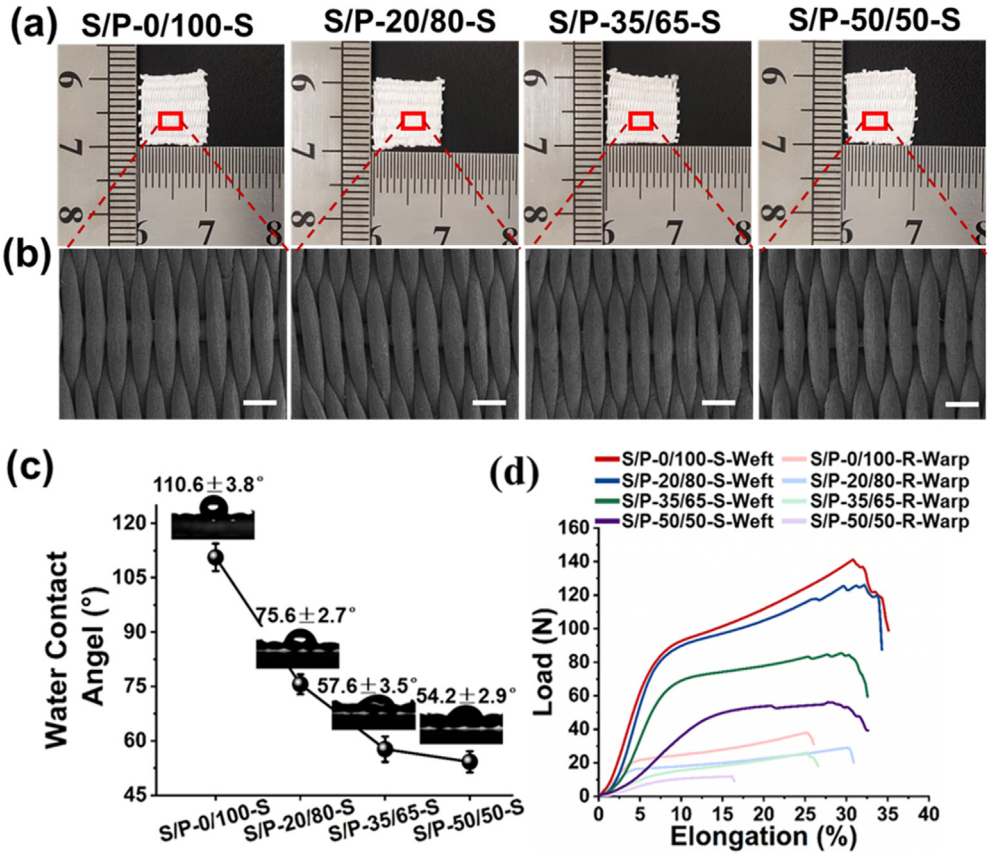

Fig. 5. Preparation and characterizations of woven fabrics using four different hot stretched SF/PLLA nanoyarns. (a) Photographs of four SF/PLLA woven fabrics. (b) SEM images of four SF/PLLA woven fabrics. Scale bars = 0.5 mm. (c) Water contact angel data of four SF/PLLA woven fabrics. (d) Representative load–elongation curves along weft and warp directions of four SF/PLLA woven fabrics.

20/80-S woven fabric, 0.928 ± 0.077 mm^2 for S/P-35/65-S woven fabric, 0.944 ± 0.107 mm^2 for S/P-50/50-S woven fabric, respectively. No significant difference was found among each group. The results from the water contact angel test showed that the S/P-0/100-S woven fabric exhibited obvious hydrophobic property with a water contact angle of 110.6 ± 3.8°. As comparison, the incorporation of SF improved the hydrophilicity (Fig. 5(c)). The water contact angel of S/P-20/80-S, S/P-35/65-S, and S/P-50/50-S woven fabrics were determined to be 75.6 ± 2.7°, 57.7 ± 3.5° and 54.2 ± 2.9°, respectively, demonstrating that the increase of SF/PLLA mass ratio decreased the contact angle of nanotextiles. The four different SF/PLLA woven fabrics were found to possess notably anisotropic mechanical properties (Fig. 5(d)). The breaking load, ultimate strength and Young's modulus in the weft direction were obviously higher than those in the warp direction (Supplemental Fig. S4(a)–(d)), because the yarn density along with the weft direction was notably higher than that along with the warp direction in the weaving pattern. The yarn density was a key factor determining the mechanical performances of woven fabrics. Moreover, the mechanical properties of woven fabrics largely depended on the material component of nanoyarns, and increasing the SF/PLLA mass ratio dramatically decreased the mechanical properties of finally obtained woven textiles, which was consistent with the above-mentioned testing results of mechanical properties of nanoyarns. One previous study fabricated polyacrylonitrile (PAN) nanonyarn-based woven scaffolds, which exhibited a failure stress of ~3 MPa and a Young's modulus of ~1 MPa [4]. Another study fabricated polycaprolactone (PCL) nanoyarn-based woven scaffolds, which possessed a failure stress of ~10 MPa and Young's modulus of ~60 MPa [45]. With the continuous technical advances, the failure stress of different SF/PLLA nanoyarn-based woven scaffolds fabricated in our study was in the range of 15–30 MPa, and the Young's modulus ranged from 90 to 310 MPa.

Appropriate biological properties were another key factor for the development of ideal elecrospun nanoyarns [51–53]. The HADMSCs were chosen as the model cells and seeded on the four SF/PLLA nanoyarn-based woven fabrics, to investigate how the scaffold component and structure affected the cell activities (Fig. 6(a)). An IFluorTM 488

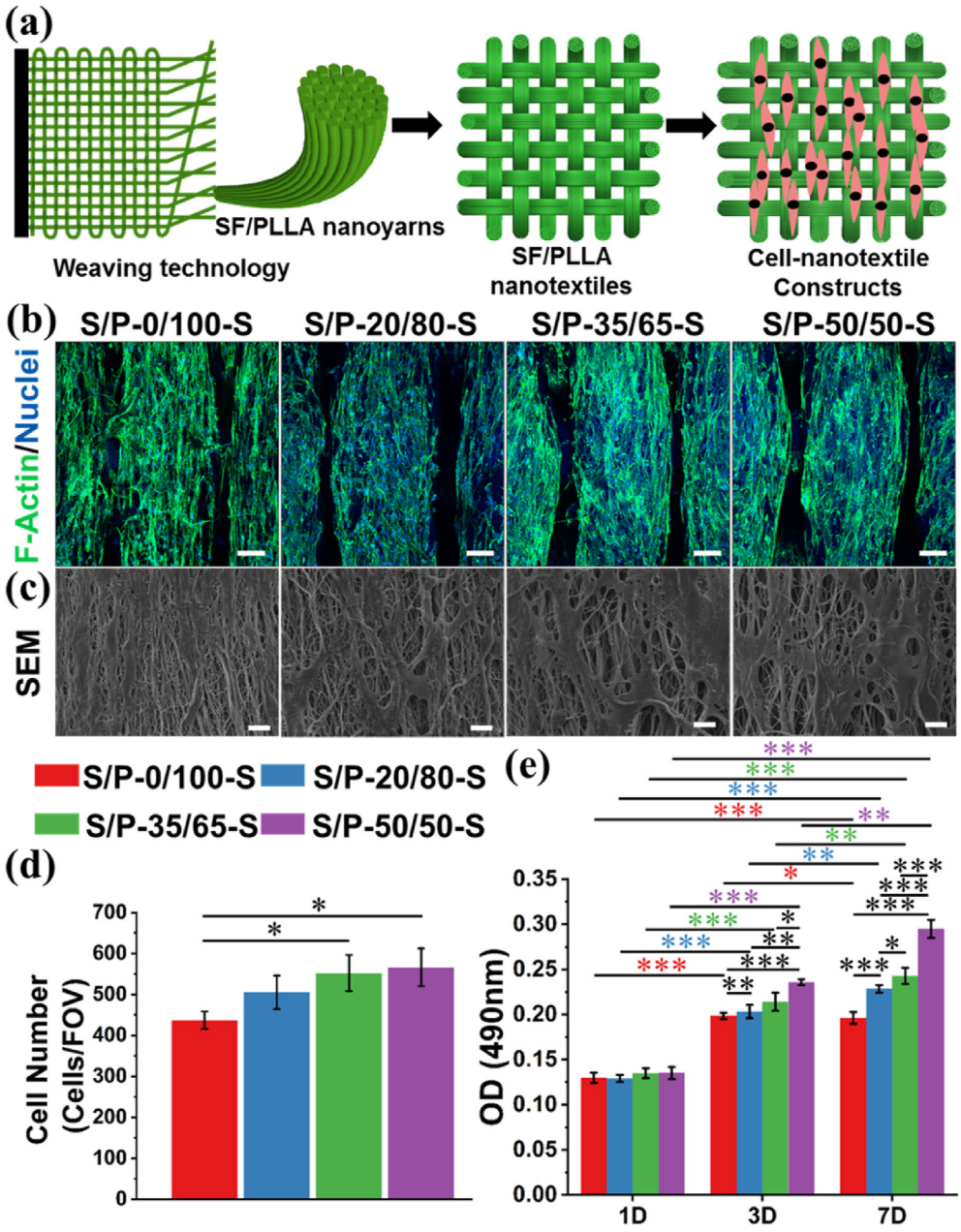

Fig. 6. *In vitro* characterizations of HADMSCs seeded on different SF/PLLA nanoyarn-based woven fabrics after 7 days of culture. (a) Design of the cell seeding and culture experiment. (b) F-actin (green) and nuclei (blue) immunofluorescent staining of HADMSCs cultured on different SF/PLLA woven fabrics at day 7. Scale bars = 100 μm. (c) SEM images of HADMSCs cultured on different SF/PLLA woven fabrics at day 7. Scale bars = 50 μm. (d) Quantitative analysis of cell number after 7 days of culture (n = 3; *p < 0.05). (e) MTT assay results of HADMSCs cultured on different woven fabrics throughout 7 days (n = 5; *p < 0.05, **p < 0.001, ***p < 0.0001). (For interpretation of the references to color in this figure legend, the reader is referred to the Web version of this article.)

phalloidin and DAPI double-staining method was employed to visualize the cytoskeleton (green) and nuclei (blue) of HADMSCs seeded on the four different woven fabrics after 7 days of culture (Fig. 6(b) and Supplemental Fig. S5). The results showed that the HADMSCs exhibited spindle-like shape and remolded their shape parallel to the fiber alignment direction on all the four woven fabrics. The statistical analysis showed that the cell number on both S/P-35/65-S and S/P-50/50-S woven fabrics was significantly higher than the S/P-0/100-S woven fabric (Fig. 6(c)). SEM images of HADMSC-woven fabric constructions also confirmed that the cells adhered and grew well on all the four woven fabrics, and the nanofibers in the woven fabrics could regulate the cellular shape through contact guidance (Fig. 6(d)). A MTT assay was

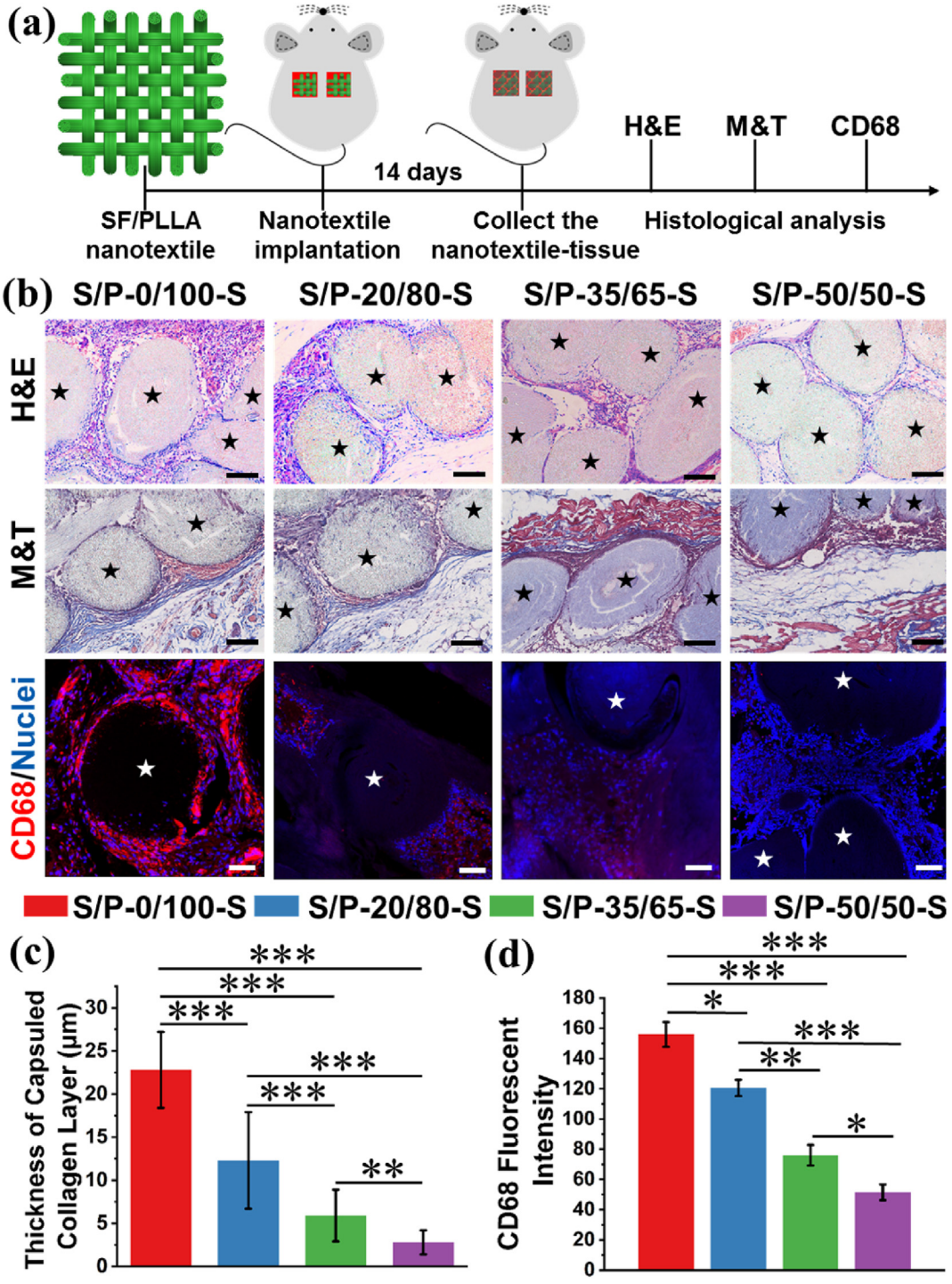

Fig. 7. Inflammatory response of different SF/PLLA nanoyarn-based woven fabrics after 14 days of subcutaneous implantation. (a) Design of the subcutaneous implantation experiment. (b) H&E staining, M&T staining and CD68 (red) immunofluorescent staining of different SF/PLLA woven fabrics after subcutaneously implanted in rat for 14 days. Blue fluorescent was utilized to visualize the nuclei for immunofluorescent staining. The pentacles stand for nanoyarns existed in the woven fabrics. Scale bars for H&E staining and M&T staining: 100 μm. Scale bars for immunofluorescent staining: 50 μm. (c) Quantitative analysis of thickness of dense collagen layer surrounding the implanted textiles (n = 3; **p < 0.001, ***p < 0.0001). (d) Quantitative analysis of CD68 intensity inside the different SF/PLLA woven fabrics (n = 3; *p < 0.05, **p < 0.001, ***p < 0.0001). (For interpretation of the references to color in this figure legend, the reader is referred to the Web version of this article.)

utilized to characterize the proliferation behavior of HADMSCs seeded on the four different woven fabrics throughout 7 days of culture (Fig. 6(e)). It was found that all the four different woven fabrics showed the similar optical density (OD) value with no significant differences at day 1. With increasing the culture time, the OD value among the four different woven fabrics exhibited obvious differences. The S/P-50/50-S nanoyarn-based woven fabric showed highest OD value and the S/P-0/100-S nanoyarn-based woven fabric presented lowest OD value at day 3 and day 7, indicating that the introduction of SF bioactive component was assuredly beneficial for the cell proliferation, and the cell proliferation capacity significantly improved with the increase of SF/PLLA mass ratio. Taken together, the SF/PLLA nanoyarn-based woven fabrics could provide an instructive bio-environment to enhance the cell attachment, alignment, and proliferation.

Controlling and regulating the stem cell differentiation is also significant importance for biomaterial scaffolds. Our previous studies have demonstrated that the nanoyarns themselves could not promote the differentiation of HADMSCs, but the nanoyarns could support the biochemical induction of HADMSC differentiation toward smooth muscle,Schwann cells, osteogenic and tenogenic lineages by using the corresponding differentiation medium [4,45,54]. Moreover, our previous study and existing studies from other groups also indicated that the loading of bioactive agents like therapeutic drugs and cytokines into nanoyarns are simple and feasible for inducing the directional differentiation of stem cells [32,55,56]. Therefore, the bioactive agents will be considered to be encapsulated into the SF/PLLA nanoyarns to induce and guide the directional differentiation of HADMSCs in our future work.

3.5. *In vivo subcutaneous implantation of SF/PLLA nanoyarn-based woven fabrics*

Four types of nanoyarn-based woven fabrics with different SF/PLLA mass ratios were further implanted subcutaneously in the rat model to explore the inflammatory response *in vivo* (Fig. 7(a)). The images of H&E staining showed that the cells from host tissue infiltrated into the gaps between adjacent nanoyarns and penetrated throughout the whole scaffolds to form a tissue-scaffold complex after 14 days of implantation for all the SF/PLLA nanoyarn-based woven fabrics (Fig. 7(b), upper panel). The obvious SF/PLLA nanoyarns can be found in the cross-sectional slides. The images of M&T staining showed that the obvious collagen deposition was detected on the surface of the woven fabrics and a few scattered collagen fibers was found in the gaps between adjacent nanoyarns in the woven fabrics after 14 days of implantation for all the SF/PLLA nanoyarn-based woven fabrics (Fig. 7(b), middle panel). The statistical analysis showed that the thickness of surrounded dense collagen layer was highest for S/P-0/100-S woven fabric, and the lowest collagen thickness was found for S/P-50/50-S woven fabric (Fig. 7(c)). The immunofluorescence staining of CD68 protein (one general marker for macrophage) was conducted to visualize the inflammatory response in the four different woven fabrics with diverse SF/PLLA mass ratios (Fig. 7(b), bottom panel). It was found that the highest level of CD68 protein expression was found in the S/P-0/100-S nanoyarn-based woven fabric, and the expression level of CD68 protein seemed to present a gradually decreased trend with the increase of SF/PLLA mass ratio. Quantitative calculation of fluorescent intensity of CD68 protein confirmed that the inflammatory response decreased notably with the increase of SF/PLLA mass ratio (Fig. 7(d)). All these results demonstrated that the SF/PLLA nanoyarn-based woven fabrics effectively promoted the cellular infiltration and tissue regeneration *in vivo*, and the inflammatory response dramatically reduced by the introduction of bioactive SF component.

It is well known that the macrophages and other immune cells usually are recruited to the implantation sites and trigger an inflammatory response, when a foreign man-made scaffold is implanted into the body [9,57,58]. Therefore, the ideal engineered scaffolds should promote the regeneration of damaged tissues and reduce the inflammatory response. In our present study, four hot stretched SF/PLLA nanoyarns were fabricated into woven fabrics and were future implanted subcutaneously in the rat model. The results demonstrated that the controlled porous structure of woven fabrics was positively conducive for the cell infiltration and tissue regeneration *in vivo*. Some other studies also demonstrated that the woven fabrics with controllable pore size and porosity could significantly promote the cell penetration into the whole woven patterns, further forming the 3D tissue architecture and structure [38,59]. Importantly, this study also demonstrated that all the four woven textiles with different SF/PLLA mass ratios could trigger the inflammatory response, but the woven textiles with higher SF component had less fibrosis structure and less recruited macrophages. Taken together, our study demonstrated the feasibility of controlling and regulating the morphology, structure, biodegradability, and mechanical properties as well as biological properties of the nanoyarns by adjusting the SF/PLLA mass ratios. Eventually, it is envisioned that our SF/PLLA nanoyarns and their fascinated woven textiles were potential candidates for the soft tissue engineering applications.

4. Conclusion

In this study, one electrospinning nanoyarn-forming unit and one hot stretching unit was integrated to fabricate high performance SF/PLLA nanoyarns. We systematically explored how the hot stretching process and SF/PLLA mass ratio influenced the morphology, structure, and mechanical properties of the as-developed nanoyarns. It was found that the hot stretched nanoyarns exhibited obviously higher fiber alignment, crystallinity, and mechanical performances in comparison with the unstretched nanoyarns. Moreover, increasing the SF/PLLA mass ratio was found to significantly decrease the crystallinity and mechanical properties, but obviously increase the surface hydrophilicity and degradation rate of nanoyarns. The *in vitro* cell experiments manifested that the woven fabrics with more SF component were more beneficial to promote the attachment, growth, and proliferation of HADMSCs. Importantly, the *in vivo* subcutaneous implantation showed that the autologous cells penetrated and infiltrated throughout all the SF/PLLA woven fabrics, and increasing the SF component apparently mitigated the inflammatory response of the corresponding woven fabrics. This study indicated that the engineered SF/PLLA nanoyarns with tunable mechanical and biological properties would potentially be suitable for the construction of various textile-based tissue scaffolds.

Credit author statement

Jiao Liu: Methodology, Investigation, Writing-original draft. **Tao Li:** Methodology, Investigation. **Hao Zhang:** Investigation. **Wenwen Zhao:** Methodology. **Lijun Qu:** Methodology, Writing-review & editing. **Shaojuan Chen:** Methodology, Writing-review & editing. **Shaohua Wu:** Conceptualization, Methodology, Writing-review & editing, Supervision. All authors have read and agreed to the published version of the manuscript.

Data availability statement

The raw/processed data required to reproduce these findings cannot be shared at this time as the data also forms part of an ongoing study.

Declaration of competing interest

The authors declare that they have no known competing financial interests or personal relationships that could have appeared to influence the work reported in this paper.

Acknowledgments

This work has been supported by Shandong Science Foundation for

Young Scholar (ZR2020QE090), and Start-up Grant of Qingdao University.

Appendix A. Supplementary data

Supplementary data to this article can be found online at https://doi.org/10.1016/j.mtbio.2022.100243.

References

[1] C. Jiang, K. Wang, Y. Liu, C. Zhang, B. Wang, Application of textile technology in tissue engineering: a review, Acta Biomater 128 (2021) 60–76, https://doi.org/10.1016/j.actbio.2021.04.047.

[2] Y. Jiao, C. Li, L. Liu, F. Wang, X. Liu, J. Mao, L. Wang, Construction and application of textile-based tissue engineering scaffolds: a review, Biomater. Sci. 8 (2020) 3574–3600, https://doi.org/10.1039/d0bm00157k.

[3] W. Shao, J. He, Q. Han, F. Sang, Q. Wang, L. Chen, S. Cui, B. Ding, A biomimetic multilayer nanofiber fabric fabricated by electrospinning and textile technology from polylactic acid and Tussah silk fibroin as a scaffold for bone tissue engineering, Mater. Sci. Eng. C-Mater. Biol. Appl. 67 (2016) 599–610, https://doi.org/10.1016/j.msec.2016.05.081.

[4] S. Wu, Y. Wang, P.N. Streubel, B. Duan, Living nanofiber yarn-based woven biotextiles for tendon tissue engineering using cell tri-culture and mechanical stimulation, Acta Biomater 62 (2017) 102–115, https://doi.org/10.1016/j.actbio.2017.08.043.

[5] J. Liu, H. Zhai, Y. Sun, S. Wu, S. Chen, Developing high strength poly(L-lactic acid) nanofiber yarns for biomedical textile materials: a comparative study of novel nanofiber yarns and traditional microfiber yarns, Mater. Lett. 300 (2021) 130229, https://doi.org/10.1016/j.matlet.2021.130229.

[6] S. Wu, J. Liu, J. Cai, J. Zhao, S. Chen, B. Duan, Combining electrospinning with hot drawing process to fabricate high performance poly (L-lactic acid) nanofiber yarns for advanced nanostructured bio-textiles, Biofabrication 13 (2021), 045018, https://doi.org/10.1088/1758-5090/ac2209.

[7] G.Z. Tan, Y. Zhou, Electrospinning of biomimetic fibrous scaffolds for tissue engineering: a review, Int. J. Polym. Mater. Polym. Biomat. 69 (2019) 947–960, https://doi.org/10.1080/00914037.2019.1636248.

[8] G. Jin, R. He, B. Sha, W. Li, H. Qing, R. Teng, F. Xu, Electrospun three-dimensional aligned nanofibrous scaffolds for tissue engineering, Mater. Sci. Eng. C-Mater. Biol. Appl. 92 (2018) 995–1005, https://doi.org/10.1016/j.msec.2018.06.065.

[9] J.G. Snedeker, J. Foolen, Tendon injury and repair-A perspective on the basic mechanisms of tendon disease and future clinical therapy, Acta Biomater 63 (2017) 18–36, https://doi.org/10.1016/j.actbio.2017.08.032.

[10] L. Gaut, D. Duprez, Tendon Development and Diseases, vol. 5, Wiley Interdiscip Rev Dev Biol., 2016, pp. 5–23, https://doi.org/10.1002/wdev.201.

[11] F. Dormont, M. Varna, P. Couvreur, Nanoplumbers: biomaterials to fight cardiovascular diseases, Mater. Today 21 (2018) 122–143, https://doi.org/10.1016/j.mattod.2017.07.008.

[12] M. Rodriguez, J.A. Kluge, D. Smoot, M.A. Kluge, D.F. Schmidt, C.R. Paetsch, P.S. Kim, D.L. Kaplan, Fabricating mechanically improved silk-based vascular grafts by solution control of the gel-spinning process, Biomaterials 230 (2020) 119567, https://doi.org/10.1016/j.biomaterials.2019.119567.

[13] Y. Jia, W. Yang, K. Zhang, S. Qiu, J. Xu, C. Wang, Y. Chai, Nanofiber arrangement regulates peripheral nerve regeneration through differential modulation of macrophage phenotypes, Acta Biomater 83 (2019) 291–301, https://doi.org/10.1016/j.actbio.2018.10.040.

[14] B. Sun, Z. Zhou, D. Li, T. Wu, H. Zheng, J. Liu, G. Wang, Y. Yu, X. Mo, Polypyrrole-coated poly(l-lactic acid-co-epsilon-caprolactone)/silk fibroin nanofibrous nerve guidance conduit induced nerve regeneration in rat, Mater. Sci. Eng. C-Mater. Biol. Appl. 94 (2019) 190–199, https://doi.org/10.1016/j.msec.2018.09.021.

[15] Y. Zhang, Z. Zhang, Y. Wang, Y. Su, M. Chen, 3D myotube guidance on hierarchically organized anisotropic and conductive fibers for skeletal muscle tissue engineering, Mater. Sci. Eng. C-Mater. Biol. Appl. 116 (2020) 111070, https://doi.org/10.1016/j.msec.2020.111070.

[16] S. Jana, S.K. Levengood, M. Zhang, Anisotropic materials for skeletal-muscle-tissue engineering, Adv. Mater. 28 (2016) 10588–10612, https://doi.org/10.1002/adma.201600240.

[17] F. Göktepe, B.B. Mülayim, Long path towards to success in electrospun nanofiber yarn production since 1930's: a critical review, Autex Res. J. 18 (2018) 87–109, https://doi.org/10.1515/aut-2018-0004.

[18] B. Zhou, X. Jiang, R. Wang, X. Yuan, Y. Liu, Developments in electrospinning of nanofiber yarns, J. Phys. Conf. Ser. 1790 (2021) 12081, https://doi.org/10.1088/1742-6596/1790/1/012081.

[19] A. Sensini, L. Cristofolini, Biofabrication of electrospun scaffolds for the regeneration of tendons and ligaments, Materials 11 (2018) 1963, https://doi.org/10.3390/ma11101963.

[20] S. Wu, S. Ni, X. Jiang, M.A. Kuss, H.J. Wang, B. Duan, Guiding mesenchymal stem cells into myelinating Schwann cell-like phenotypes by using electrospun core-sheath nanoyarns, ACS Biomater. Sci. Eng. 5 (2019) 5284–5294, https://doi.org/10.1021/acsbiomaterials.9b00748.

[21] M. Akbari, A. Tamayol, S. Bagherifard, L. Serex, P. Mostafalu, N. Faramarzi, M.H. Mohammadi, A. Khademhosseini, Textile technologies and tissue engineering: a path toward organ weaving, Adv. Healthc. Mater. 5 (2016) 751–766, https://doi.org/10.1002/adhm.201500517.

[22] J. Xiong, P.S. Lee, Progress on wearable triboelectric nanogenerators in shapes of fiber, yarn, and textile, Sci. Technol. Adv. Mater. 20 (2019) 837–857, https://doi.org/10.1080/14686996.2019.1650396.

[23] X. Zhou, S. Fang, X. Leng, Z. Liu, R.H. Baughman, The power of fiber twist, Acc. Chem. Res. 54 (2021) 2624–2636, https://doi.org/10.1021/acs.accounts.1c00112.

[24] W.-E. Teo, R. Gopal, R. Ramaseshan, K. Fujihara, S. Ramakrishna, A dynamic liquid support system for continuous electrospun yarn fabrication, Polymer 48 (2007) 3400–3405, https://doi.org/10.1016/j.polymer.2007.04.044.

[25] H. Maleki, A.A. Gharehaghaji, P.J. Dijkstra, Electrospinning of continuous poly (L-lactide) yarns: effect of twist on the morphology, thermal properties and mechanical behavior, J. Mech. Behav. Biomed. Mater. 71 (2017) 231–237, https://doi.org/10.1016/j.jmbbm.2017.03.031.

[26] F. Oustadi, R. Imani, M. Haghbin Nazarpak, A.M. Sharifi, Genipin-crosslinked gelatin hydrogel incorporated with PLLA-nanocylinders as a bone scaffold: synthesis, characterization, and mechanical properties evaluation, Polym. Adv. Technol 31 (2020) 1783–1792, https://doi.org/10.1002/pat.4905.

[27] L. Liu, S. Zhang, J. Huang, Progress in modification of silk fibroin fiber, Sci. China Technol. Sci. 62 (2019) 919–930, https://doi.org/10.1007/s11431-018-9508-3.

[28] F.J. O'Brien, Biomaterials & scaffolds for tissue engineering, Mater, Today 14 (2011) 88–95, https://doi.org/10.1016/s1369-7021(11)70058-x.

[29] P. Feng, P. Wu, C. Gao, Y. Yang, W. Guo, W. Yang, C. Shuai, A multimaterial scaffold with tunable properties: toward bone tissue repair, Adv. Sci. 5 (2018) 1700817, https://doi.org/10.1002/advs.201700817.

[30] L.X.L. Yang G, Y. He, J.K. Ma, G.L. Ni, S.B. Zhou, From nano to micro to macro: electrospun hierarchically structured polymeric fibers for biomedical applications, Prog. Polym. Sci. 81 (2018) 80–113, https://doi.org/10.1016/j.progpolymsci.2017.12.003.

[31] Y. Tian, J. Zhang, J. Cheng, G. Wu, Y. Zhang, Z. Ni, G. Zhao, A poly(L-lactic acid) monofilament with high mechanical properties for application in biodegradable biliary stents, J. Appl. Polym. Sci. 138 (2020) 49658, https://doi.org/10.1002/app.49656.

[32] S. Wu, R. Zhou, F. Zhou, P.N. Streubel, S. Chen, B. Duan, Electrospun thymosin Beta-4 loaded PLGA/PLA nanofiber/microfiber hybrid yarns for tendon tissue engineering application, Mater. Sci. Eng. C-Mater. Biol. Appl. 106 (2020) 110268, https://doi.org/10.1016/j.msec.2019.110268.

[33] L. Wei, S. Wu, M. Kuss, X. Jiang, R. Sun, P. Reid, X. Qin, B. Duan, 3D printing of silk fibroin-based hybrid scaffold treated with platelet rich plasma for bone tissue engineering, Bioact. Mater. 4 (2019) 256–260, https://doi.org/10.1016/j.bioactmat.2019.09.001.

[34] S. Wu, J. Liu, Y. Qi, J. Cai, J. Zhao, B. Duan, S. Chen, Tendon-bioinspired wavy nanofibrous scaffolds provide tunable anisotropy and promote tenogenesis for tendon tissue engineering, Mater. Sci. Eng. C-Mater. Biol. Appl. 126 (2021) 112181, https://doi.org/10.1016/j.msec.2021.112181.

[35] M. Spasova, O. Stoilova, N. Manolova, I. Rashkov, Electrospun PLLA/PEG scaffolds, Mater. Today 28 (2019) 114–115, https://doi.org/10.1016/j.mattod.2019.07.001.

[36] X. Ji, W. Yang, T. Wang, C. Mao, L. Guo, J. Xiao, N. He, Coaxially electrospun core/shell structured poly(L-lactide) acid/chitosan nanofibers for potential drug carrier in tissue engineering, J. Biomed. Nanotechnol. 9 (2013) 1672–1678, https://doi.org/10.1166/jbn.2013.1665.

[37] W. Liu, Z. Li, L. Zheng, X. Zhang, P. Liu, T. Yang, B. Han, Electrospun fibrous silk fibroin/poly(L-lactic acid) scaffold for cartilage tissue engineering, Tissue Eng. Regen. Med. 13 (2016) 516–526, https://doi.org/10.1007/s13770-016-9099-9.

[38] B.B. Rothrauff, B.B. Lauro, G. Yang, R.E. Debski, V. Musahl, R.S. Tuan, Braided and stacked electrospun nanofibrous scaffolds for tendon and ligament tissue engineering, Tissue Eng. 23 (2017) 378–389, https://doi.org/10.1089/ten.TEA.2016.0319.

[39] R. Androsch, C. Schick, M.L. Di Lorenzo, Melting of conformationally disordered crystals (α′-Phase) of poly(l-lactic acid), Macromol. Chem. Phys. 215 (2014) 1134–1139, https://doi.org/10.1002/macp.201400126.

[40] L. Bai, X. Zhao, R.-Y. Bao, Z.-Y. Liu, M.-B. Yang, W. Yang, Effect of temperature, crystallinity and molecular chain orientation on the thermal conductivity of polymers: a case study of PLLA, J. Mater. Sci. 53 (2018) 10543–10553, https://doi.org/10.1007/s10853-018-2306-4.

[41] J. Li, P. Xiao, H. Li, Y. Zhang, F. Xue, B. Luo, S. Huang, Y. Shang, H. Wen, J. de Claville Christiansen, D. Yu, S. Jiang, Crystalline structures and crystallization behaviors of poly(l-lactide) in poly(l-lactide)/graphene nanosheet composites, Polym. Chem. 6 (2015) 3988–4002, https://doi.org/10.1039/c5py00254k.

[42] T. Tábi, S. Hajba, J.G. Kovács, Effect of crystalline forms (α′ and α) of poly(lactic acid) on its mechanical, thermo-mechanical, heat deflection temperature and creep properties, Eur. Polym. J. 82 (2016) 232–243, https://doi.org/10.1016/j.eurpolymj.2016.07.024.

[43] M. Yousefzadeh, M. Latifi, W.-E. Teo, M. Amani-Tehran, S. Ramakrishna, Producing continuous twisted yarn from well-aligned nanofibers by water vortex, Polym, Eng. Sci. 51 (2011) 323–329, https://doi.org/10.1002/pen.21800.

[44] A.S. Richard, R.S. Verma, Bioactive nano yarns as surgical sutures for wound healing, Mater. Sci. Eng. C-Mater. Biol. Appl. 128 (2021) 112334, https://doi.org/10.1016/j.msec.2021.112334.

[45] S. Wu, B. Duan, P. Liu, C. Zhang, X. Qin, J.T. Butcher, Fabrication of aligned nanofiber polymer yarn networks for anisotropic soft tissue scaffolds, ACS Appl. Mater. Interfaces 8 (2016) 16950–16960, https://doi.org/10.1021/acsami.6b05199.

[46] U. Ali, Y. Zhou, X. Wang, T. Lin, Direct electrospinning of highly twisted, continuous nanofiber yarns, J. Text. Inst. 103 (2012) 80–88, https://doi.org/10.1080/00405000.2011.552254.

[47] D. Li, L. Tao, Y. Shen, B. Sun, X. Xie, Q. Ke, X. Mo, B. Deng, Fabrication of multilayered nanofiber scaffolds with a highly aligned nanofiber yarn for

anisotropic tissue regeneration, ACS Omega 5 (2020) 24340–24350, https://doi.org/10.1021/acsomega.0c02554.
[48] S.H. Im, Y. Jung, Y. Jang, S.H. Kim, Poly(L-lactic acid) scaffold with oriented micro-valley surface and superior properties fabricated by solid-state drawing for blood-contact biomaterials, Biofabrication 8 (2016) 45010, https://doi.org/10.1088/1758-5090/8/4/045010.
[49] B. Yi, Y. Shen, H. Tang, X. Wang, B. Li, Y. Zhang, Stiffness of aligned fibers regulates the phenotypic expression of vascular smooth muscle cells, ACS Appl. Mater. Interfaces 11 (2019) 6867–6880, https://doi.org/10.1021/acsami.9b00293.
[50] F. Dabirian, S.A.H. Ravandi, R.H. Sanatgar, J.P. Hinestroza, Manufacturing of twisted continuous PAN nanofiber yarn by electrospinning process, Fibers Polym. 12 (2011) 610–615, https://doi.org/10.1007/s12221-011-0610-6.
[51] C. Yan, Y. Ren, X. Sun, L. Jin, X. Liu, H. Chen, K. Wang, M. Yu, Y. Zhao, Photoluminescent functionalized carbon quantum dots loaded electroactive Silk fibroin/PLA nanofibrous bioactive scaffolds for cardiac tissue engineering, J. Photochem. Photobiol., B 202 (2020) 111680, https://doi.org/10.1016/j.jphotobiol.2019.111680.
[52] S. Calamak, C. Erdogdu, M. Ozalp, K. Ulubayram, Silk fibroin based antibacterial bionanotextiles as wound dressing materials, Mater. Sci. Eng. C 43 (2014) 11–20, https://doi.org/10.1016/j.msec.2014.07.001.
[53] C. Shuai, G. Liu, Y. Yang, F. Qi, S. Peng, W. Yang, C. He, G. Wang, G. Qian, A strawberry-like Ag-decorated barium titanate enhances piezoelectric and antibacterial activities of polymer scaffold, Nano Energy 74 (2020) 104825, https://doi.org/10.1016/j.nanoen.2020.104825.
[54] S. Wu, Y. Qi, W. Shi, M. Kuss, S. Chen, B. Duan, Electrospun conductive nanofiber yarns for accelerating mesenchymal stem cells differentiation and maturation into Schwann cell-like cells under a combination of electrical stimulation and chemical induction, Acta Biomater 139 (2020) 91–104, https://doi.org/10.1016/j.actbio.2020.11.042.
[55] Y. Wang, T. Wu, J. Zhang, Z. Feng, M. Yin, X. Mo, A bilayer vascular scaffold with spatially controlled release of growth factors to enhance in situ rapid endothelialization and smooth muscle regeneration, Mater. Des. 204 (2021) 109649, https://doi.org/10.1016/j.matdes.2021.109649.
[56] C. Wang, W. Hou, X. Guo, J. Li, T. Hu, M. Qiu, S. Liu, X. Mo, X. Liu, Two-phase electrospinning to incorporate growth factors loaded chitosan nanoparticles into electrospun fibrous scaffolds for bioactivity retention and cartilage regeneration, Mater. Sci. Eng. C-Mater. Biol. Appl. 79 (2017) 507–515, https://doi.org/10.1016/j.msec.2017.05.075.
[57] S. Jin, J. Gao, R. Yang, C. Yuan, R. Wang, Q. Zou, Y. Zuo, M. Zhu, Y. Li, Y. Man, J. Li, A baicalin-loaded coaxial nanofiber scaffold regulated inflammation and osteoclast differentiation for vascularized bone regeneration, Bioact. Mater. 8 (2021) 559–572, https://doi.org/10.1016/j.bioactmat.2021.06.028.
[58] C. Shuai, W. Yang, P. Feng, S. Peng, H. Pan, Accelerated degradation of HAP/PLLA bone scaffold by PGA blending facilitates bioactivity and osteoconductivity, Bioact. Mater. 6 (2021) 490–502, https://doi.org/10.1016/j.bioactmat.2020.09.001.
[59] F. Shalchy, C. Lovell, A. Bhaskar, Hierarchical porosity in additively manufactured bioengineering scaffolds: fabrication & characterisation, J. Mech. Behav. Biomed. Mater. 110 (2020) 103968, https://doi.org/10.1016/j.jmbbm.2020.103968.